

ADVANCED MATERIALS

Supporting Information

for *Adv. Mater.*, DOI: 10.1002/adma.201504241

A Cable-Shaped Lithium Sulfur Battery

*Xin Fang, Wei Weng, Jing Ren, and Huisheng Peng**

Supporting Information

Supplementary Figures

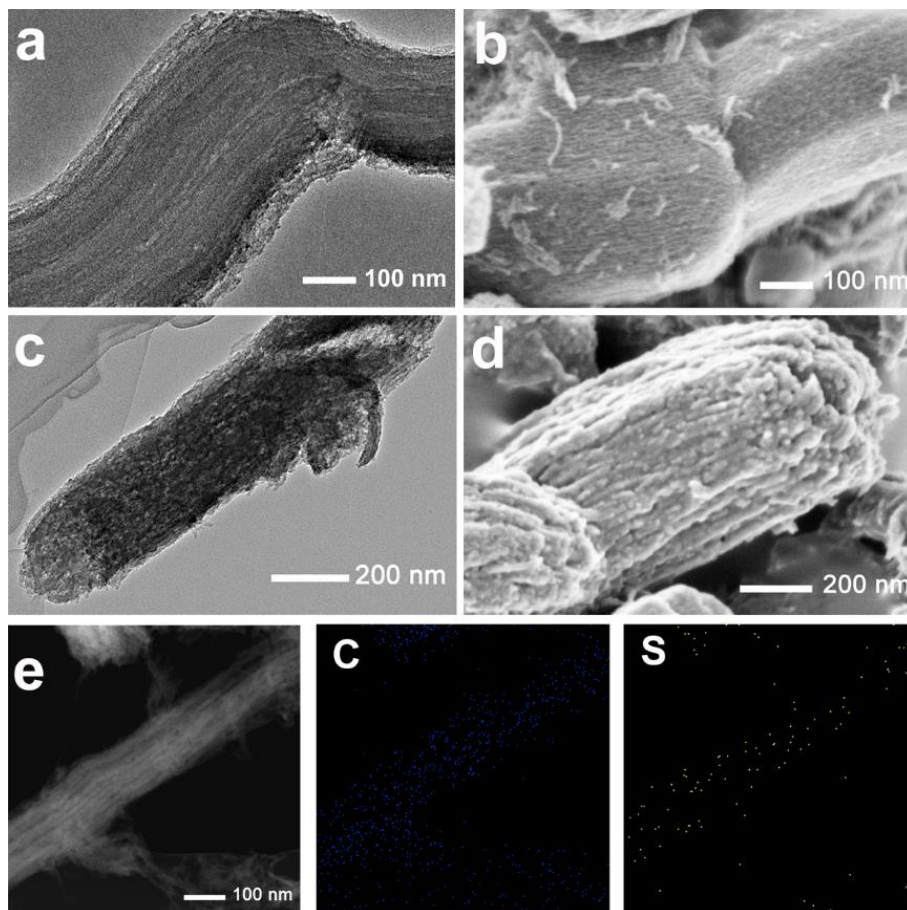


Figure S1. Morphologies of CMK-3 and CMK-3@S particles. **a** and **b**. Transmission electron microscopy (TEM) and scanning electron microscopy (SEM) images of CMK-3 particles. **c** and **d**. TEM and SEM images of CMK-3@S particles. **e**. Element mapping of a CMK-3@S particle. The left is its STEM image. The middle and the right are the distribution of carbon (blue) and sulphur (yellow) over this particle.

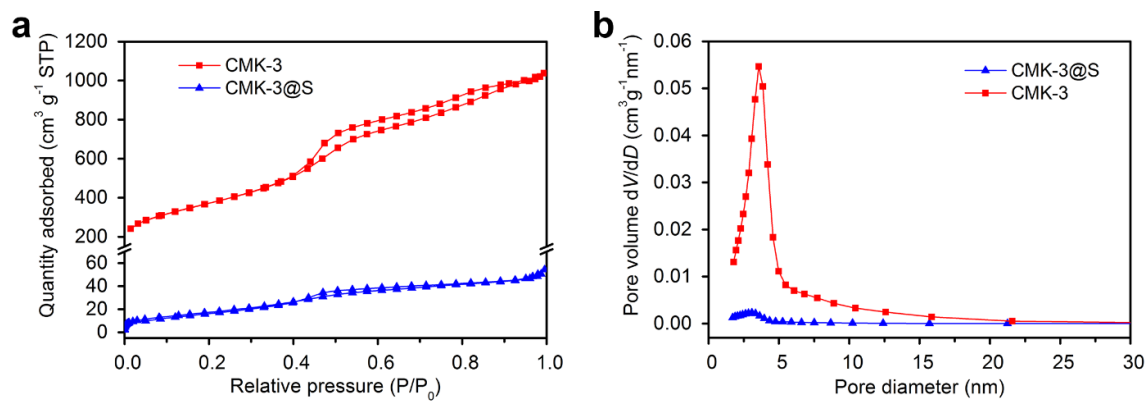


Figure S2. Brunauer-Emmett-Teller analysis of CMK-3 and CMK-3@S particles.
a. Nitrogen adsorption–desorption isotherms. **b.** Pore size distributions of CMK-3 particles before and after being imbibed with sulphur. The detail results are displayed in Table S2.

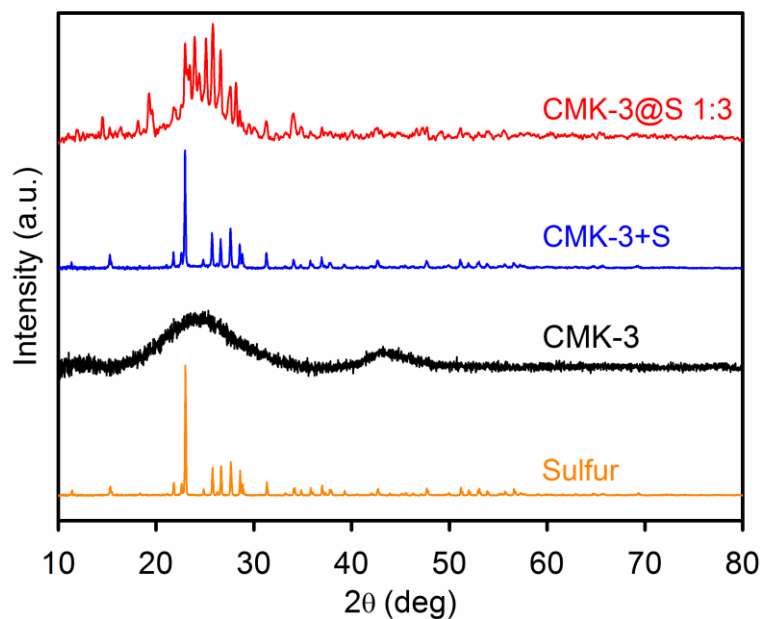


Figure S3. X-ray diffraction patterns of element sulphur, bare CMK-3, blend of CMK-3 and S and CMK-3@S particles. CMK-3+S refers to the blend of CMK-3 and element sulphur. CMK-3@S was composited by a weight ratio of S/C to be 3/1. The CMK-3@S particles exhibit a different diffraction pattern with CMK-3+S particles, indicating the sulphur was imbibed within the nanochannels of CMK-3 rather than aggregating outside.

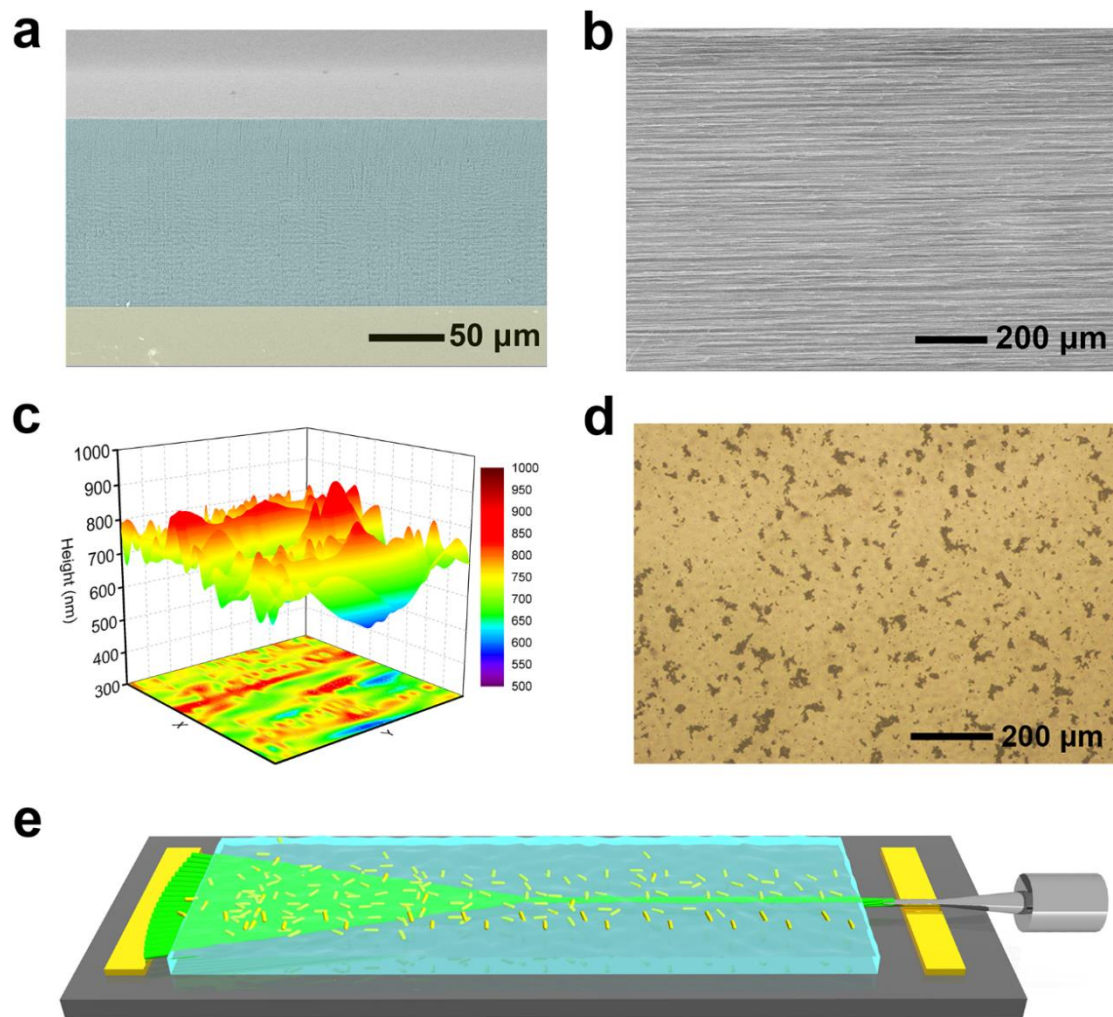


Figure S4. Preparation of carbon nanostructured hybrid fibre. **a.** SEM image of an aligned CNT array. The CNT array (light blue) was grown on a silicon wafer (light yellow) and had a height of 200 μm . **b.** SEM image of an aligned CNT sheet. **c.** The surface profile and thickness contour of 40 layers of CNT sheets that were stacked on a substrate and densified by ethanol afterwards. The 40-layer densified CNT sheets had an average thickness of ~ 760 μm . **d.** Optical micrograph of the suspension of composite particles. **e.** Schematic illustration to the preparation setup of the hybrid fibre. CNT sheets were paved on a polytetrafluoroethylene framework, immersed in suspension and twisted by an electric motor rotator.

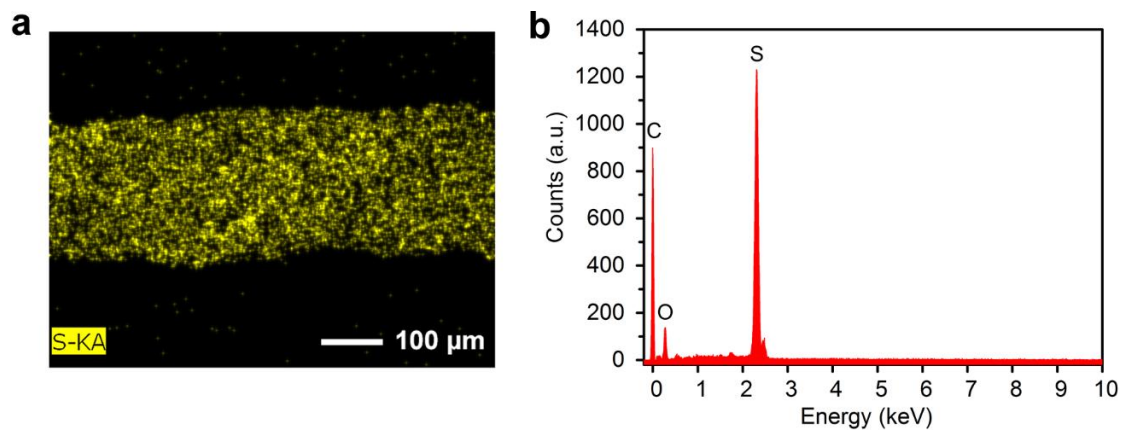


Figure S5. The element distribution of a hybrid fibre. a. Element sulphur mapping of a hybrid fibre by side view. **b.** Energy dispersive X-ray spectrum.

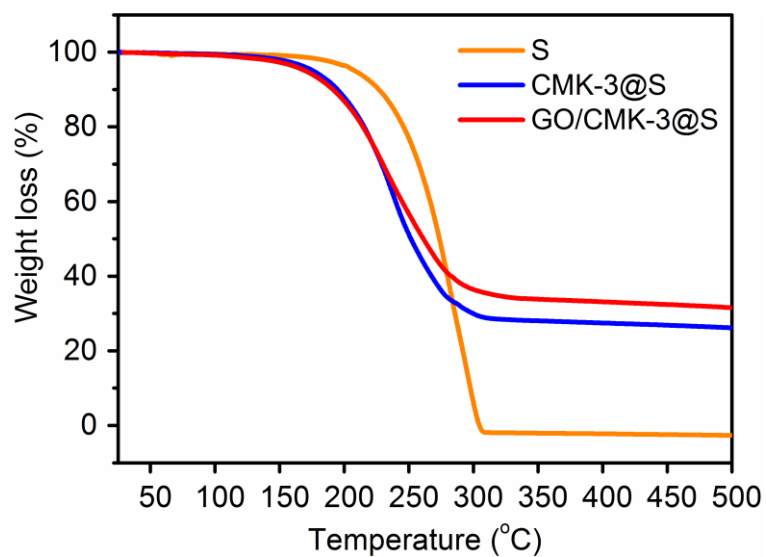


Figure S6. Thermogravimetric analysis of pristine sulphur and hybrid fibres. Since the weight loss was attributed to the vaporization of sulphur, the sulphur contents in CMK-3@S-CNT hybrid fibre and GO/CMK-3@S-CNT hybrid fibre were defined as 70 wt% and 68 wt%, respectively.

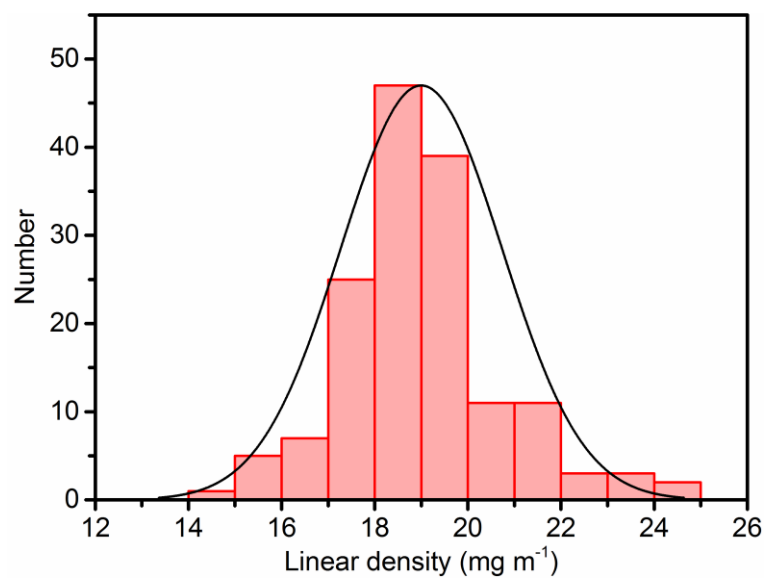


Figure S7. Histogram of linear densities of hybrid fibres. 155 samples with lengths ranging from 9–14 cm were analysed. The narrow distribution of linear density indicates a slight variability of the sulphur content in hybrid fibres.

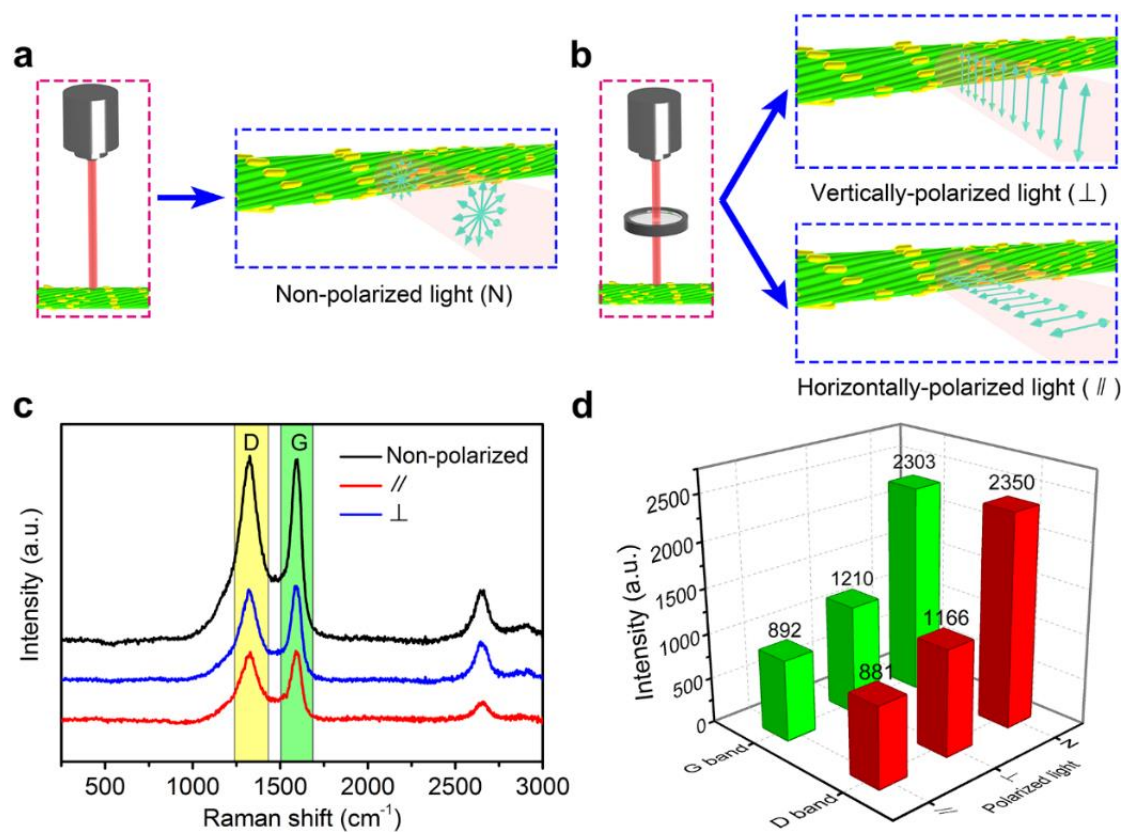


Figure S8. Polarized Raman measurement of a hybrid fibre. **a** and **b**. The schematic illustration to the polarized Raman measurement. The polarized lasers were obtained by inserting a polaroid in the light path. **c**. Raman spectra of the hybrid fibre under non-polarized and polarized lasers. **d**. The intensity of G and D bands of the hybrid fibre under non-polarized and polarized laser.

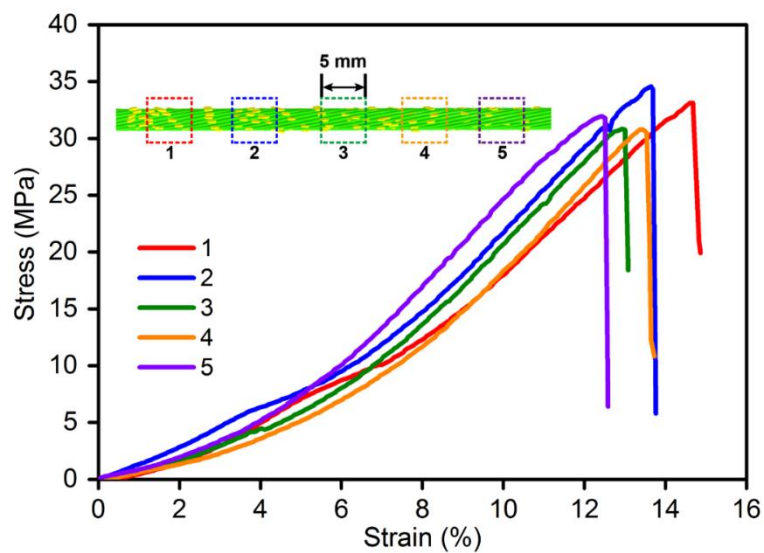


Figure S9. Stress-strain curves of a hybrid fibre. Five sections from one hybrid fibre (denoted as 1–5 in the inserted graph) were tested. Each section was 5 mm in length. The tensile strengths of different sections were 31–34 MPa, suggesting the hybrid fibre was uniform.

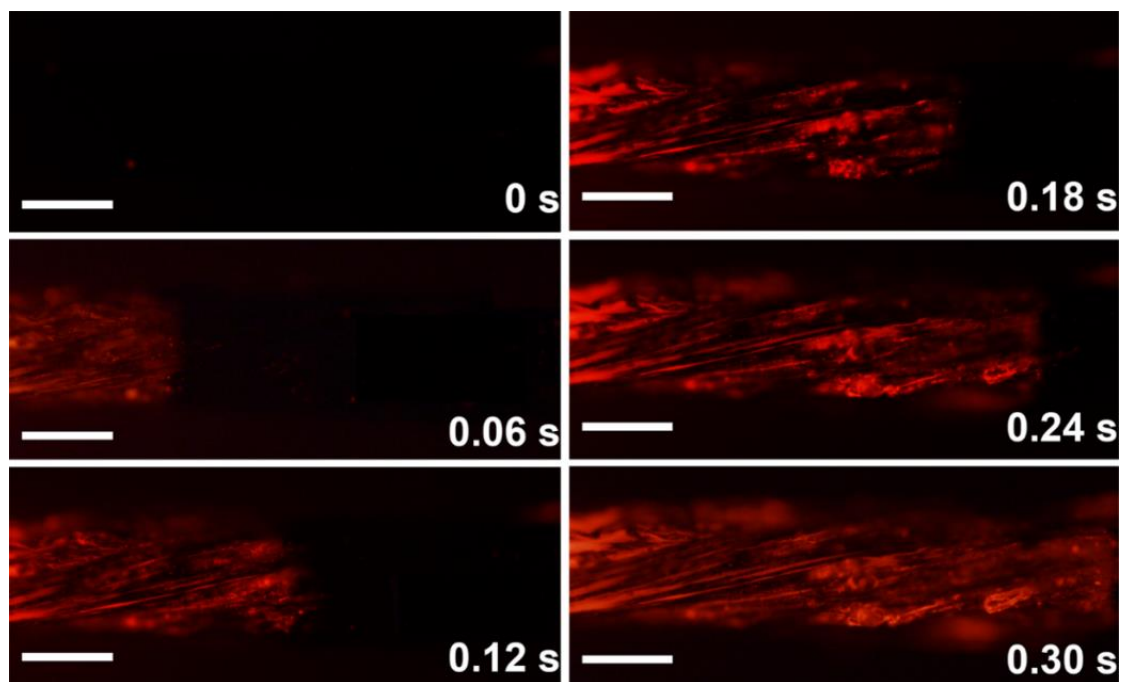


Figure S10. The infiltration of electrolyte in the hybrid fibre dynamically recorded under fluorescence microscope. 1% of rhodamine was added in the mixture solvent of DOL/DME (v/v=1/1) as an indicator. The infiltration process was recorded at a frame rate of 15 fps by the accessorial camera. Scale bars, 100 μm .

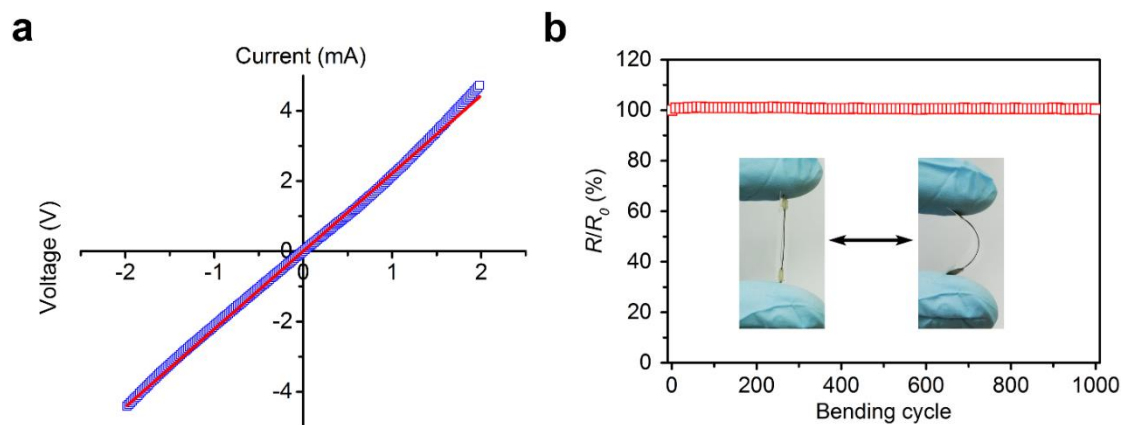


Figure S11. The electrical resistance of the hybrid fibre. **a.** Current-voltage curve of a 5-cm hybrid fibre. The scan rate of voltage was 100 mV s^{-1} . **b.** The evolution of resistance of the hybrid fibre with bending cycles. R_0 and R correspond to the resistances before and after bending, respectively. The inserted are photographs of the bending test. A 5-cm hybrid fibre was fixed on a flexible substrate with silver colloid adhesive. The bending radius was 2.5 cm.

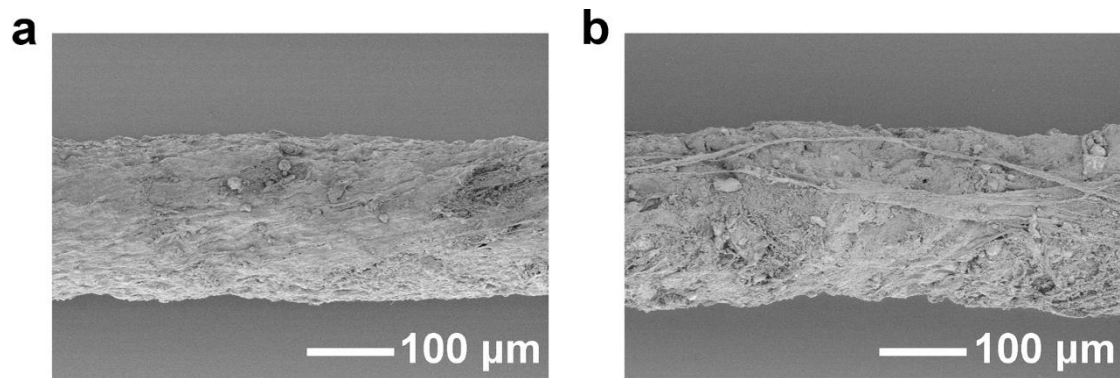


Figure S12. SEM images of a hybrid fiber before (a) and after (b) bending for 50 times (with a bending radius of 2.5 cm).

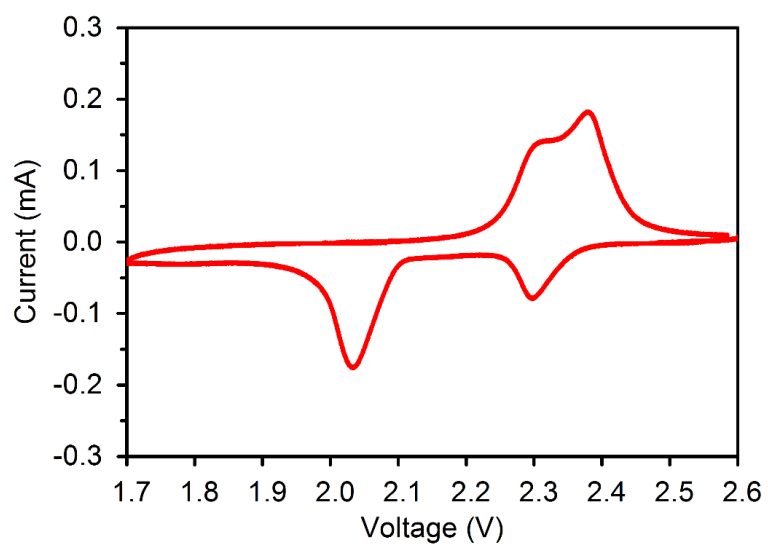


Figure S13. Cyclic voltammogram of a hybrid fibre. The scanning rate was 0.1 mV s⁻¹ within 1.7–2.6 V vs. Li/Li⁺.

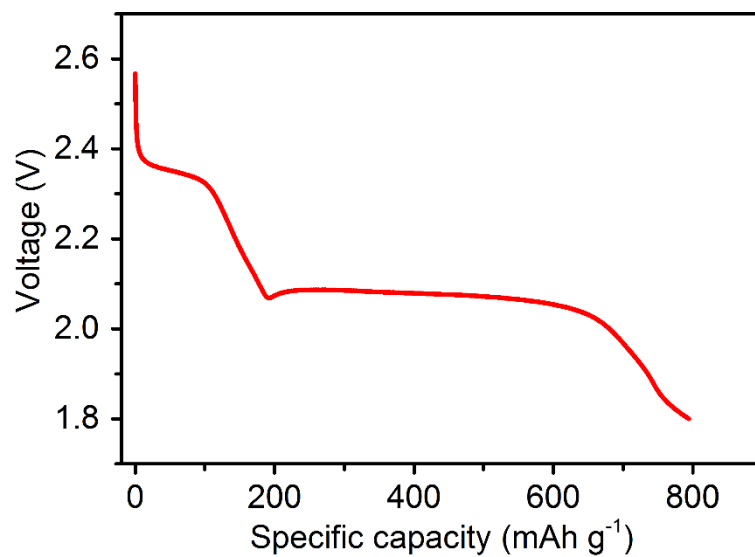


Figure S14. Galvanostatic discharge profiles of a coiled fibrous electrode. The battery was discharged from 2.4 to 1.8 V at a current rate of 0.1 C.

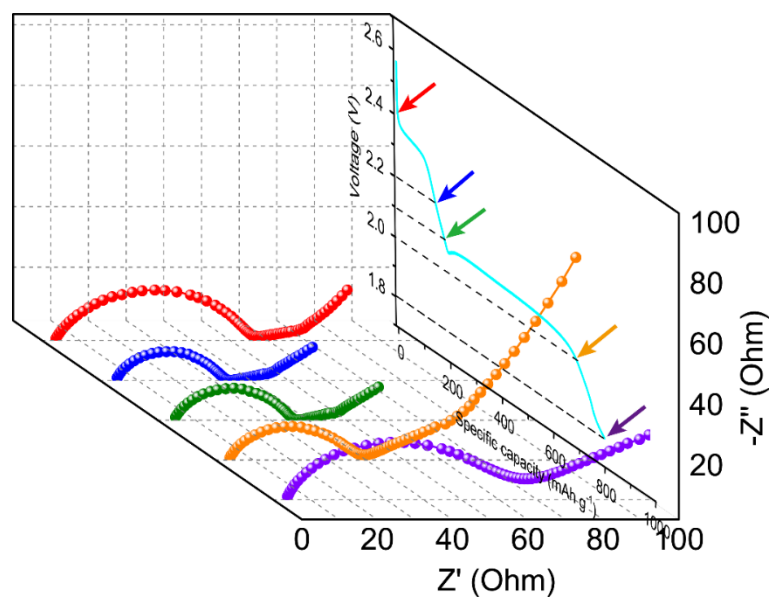


Figure S15. Electrochemical impedance spectra of a lithium sulphur battery in its discharge process. The battery was discharged from 2.4 to 1.8 V at a current rate of 0.1 C.

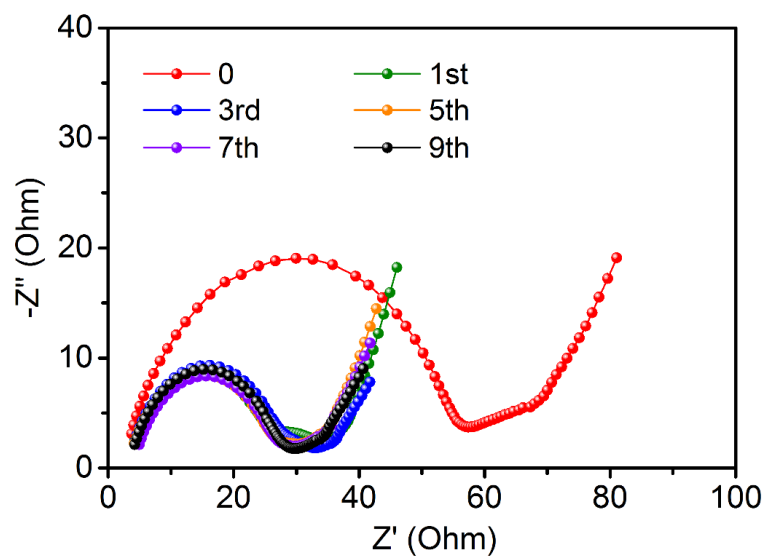


Figure S16. Electrochemical impedance spectra of a lithium sulphur battery in its initial 9 cycles. The battery was discharged and recharged between 2.6 and 1.8 V at a current rate of 1 C. The electrochemical impedance spectra was recorded at recharged state.

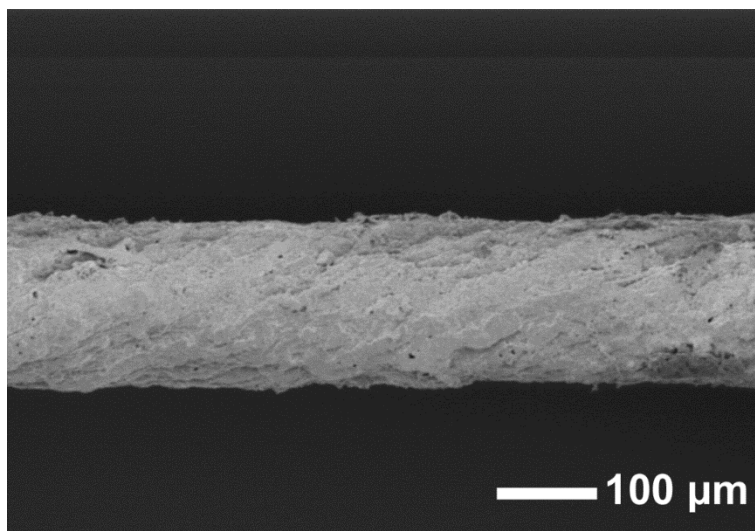


Figure S17. Morphology of a hybrid fibre cathode after cycling. The cathode had been run for 50 cycles at 0.1 C.

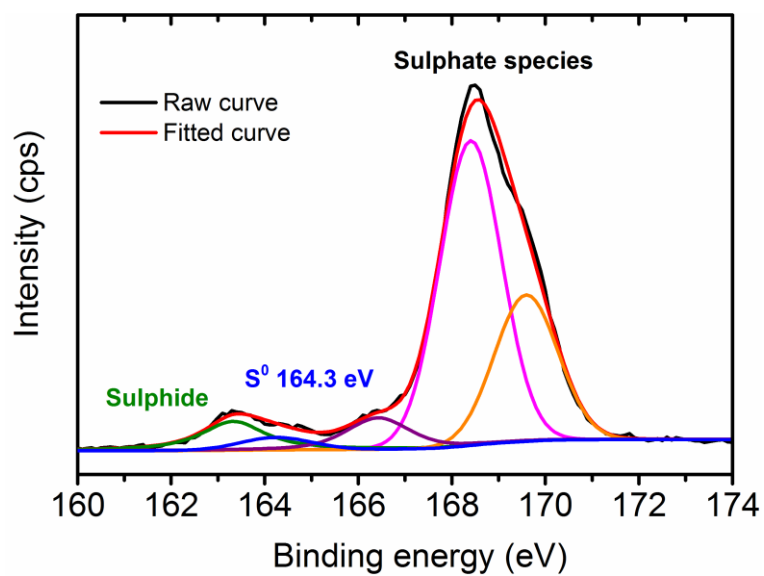


Figure S18. X-ray photoelectron spectroscopy (XPS) spectrum of the hybrid fibre cathode after cycling. The battery had been run for 50 cycles at 0.1 C and was recharged to 2.6 V. Due to the fibre-shaped configuration, the hybrid fibre was coiled for XPS examination.

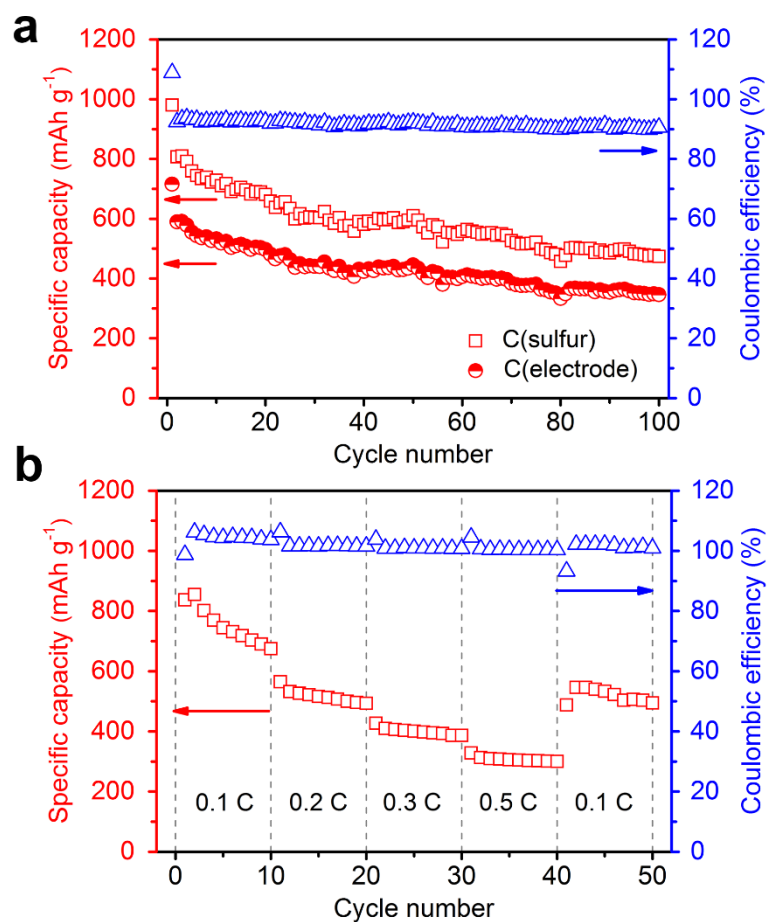


Figure S19. Cyclic and rate performances of CMK-3@S-CNT hybrid fibre. a. Discharge capacities and Coulombic efficiencies over 100 cycles at 0.1 C. **b.** Discharge capacities and Coulombic efficiencies at 0.1 C, 0.2 C, 0.3 C, 0.5 C and 0.1 C.



Figure S20. Open-circuit voltage of a cable-shaped lithium sulphur battery.

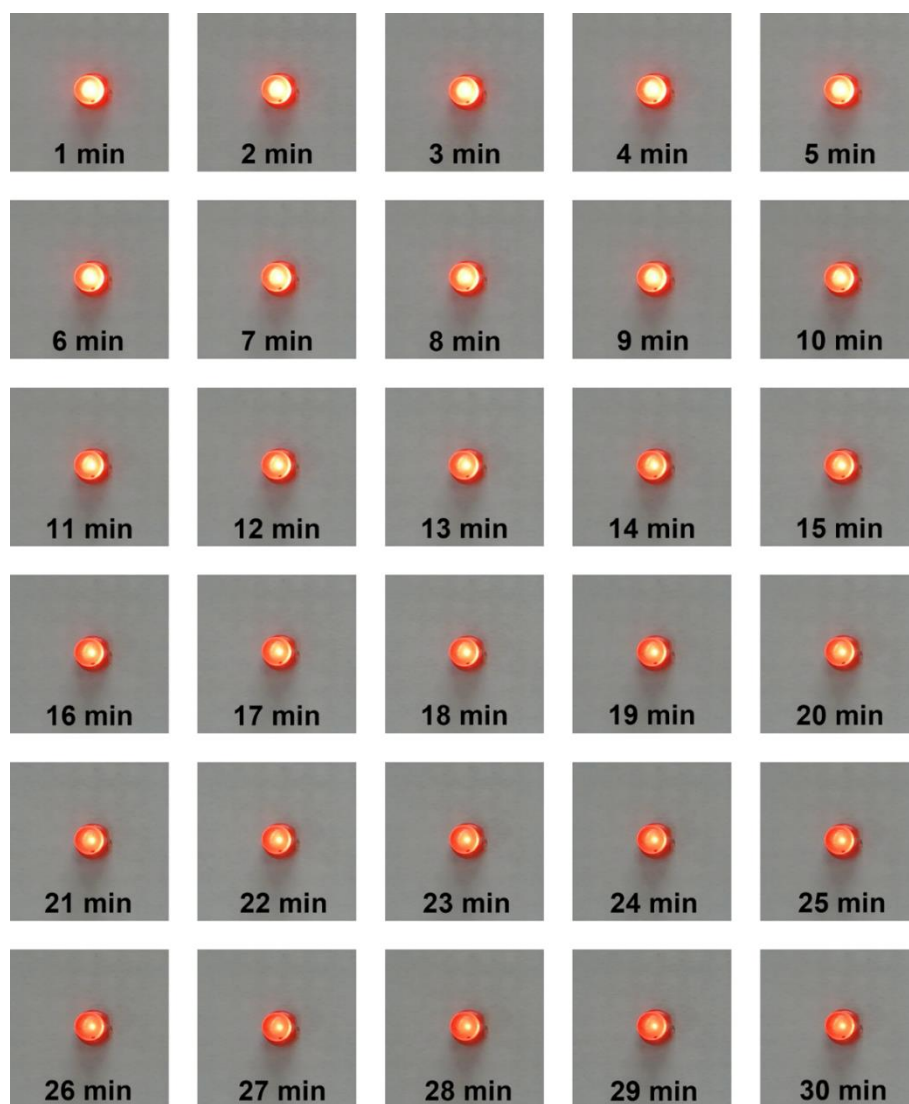


Figure S21. Photographs of a lighted red light-emitting diode (LED) in 30 min. The LED was powered by a 10-cm hybrid fibre cathode in cable-shaped lithium sulphur battery.



Figure S22. Photographs of an energy fabric. The fabric was integrated with 5 cable-shaped lithium sulphur batteries that were serially connected.

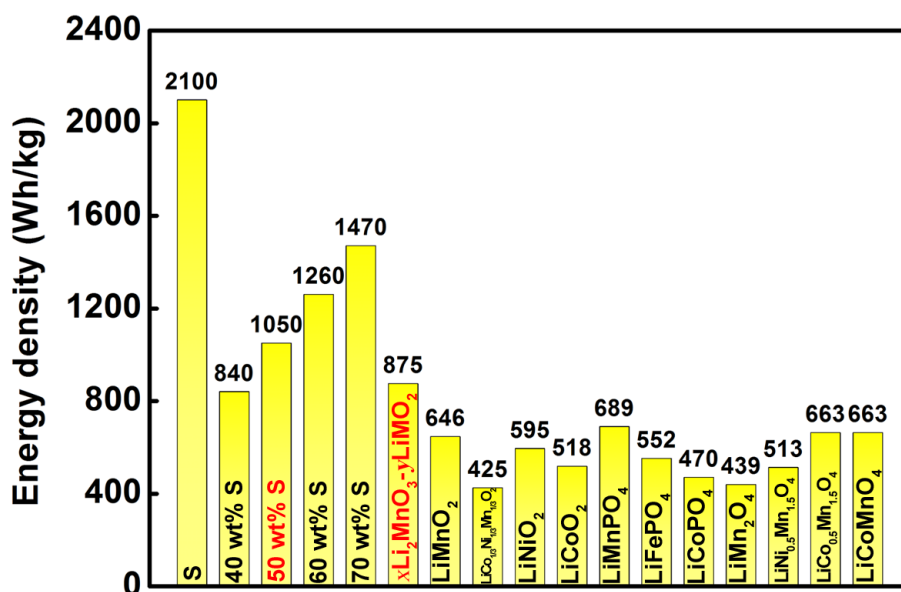


Figure S23. Practical energy densities of sulphur cathodes and representative lithium ion cathodes. The practical energy density (Wh kg^{-1}) was calculated by multiplying practical capacity (mAh g^{-1}) and the voltage plateau (V). For sulphur cathodes, their practical capacity was estimated as 1000 mAh g^{-1} given its degradation during cycling and the voltage plateau was defined as 2.1 V. The graph was re-drafted from data summarized in ref. [S1].

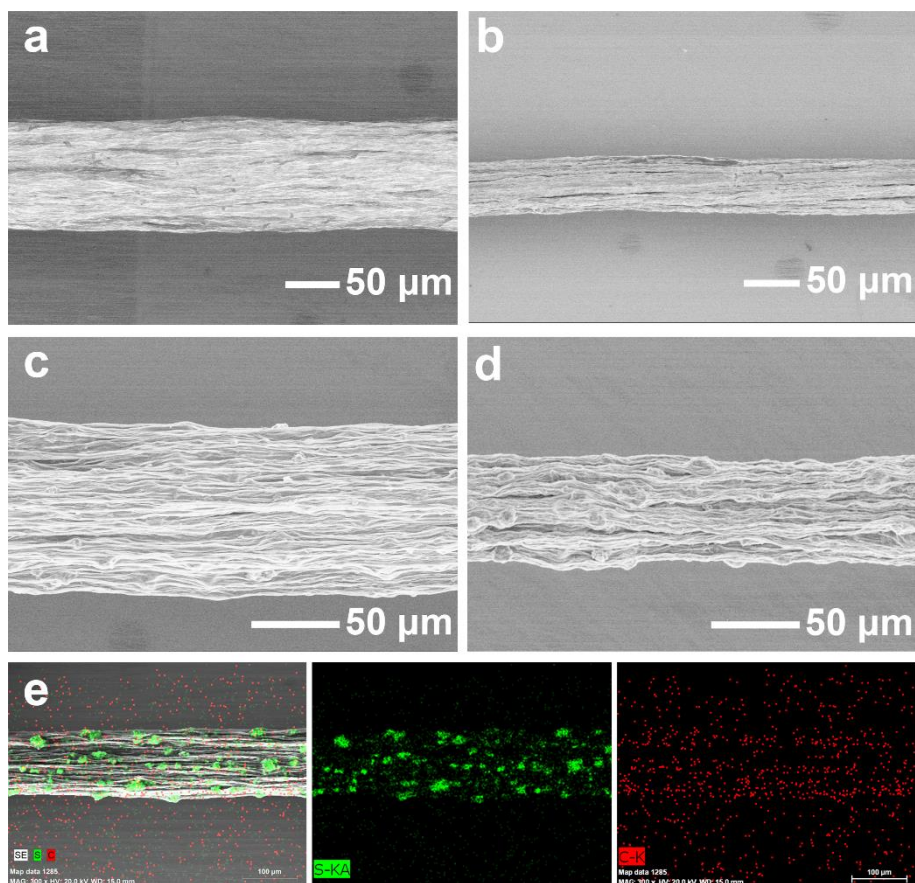


Figure S24. Morphologies of CMK-3@S-graphene hybrid fibre. a. GO fibre. **b.** Reduced GO (RGO) fibre. **c.** CMK-3@S-GO fibre. **d.** CMK-3@S-RGO fibre. **e.** Element mapping of sulphur and carbon of a CMK-3@S-GO fibre.

Supplementary Note 1

Comparison of energy densities. The energy densities of batteries displayed in Fig. 4b are specified to the total weight of the cathode containing the active materials, binder and conducting agent. The weight of current collector is not included. Energy densities are obtained by multiplying the capacity and the voltage plateau. The voltage plateaus for lithium sulphur battery and lithium silicon battery are estimated as 2.1 V and 0.3 V, respectively. For planar and cable-shaped lithium sulphur batteries, the specific capacities at the 10th cycle are adopted to rule out the capacity slump and active process at initial cycles. The planar lithium sulphur batteries displayed in Fig. 4b are listed in Table S4. Specific capacities at low rate (< 0.2 C) are used to calculate their energy densities. The gravimetric energy densities of supercapacitors are collected from ref. [S2-10]. Due to the inconsistency in units, some reports using volumetric energy densities are not included (ref. [S11-14]). Here, the gravimetric energy densities are calculated through the following equation [S15]:

$$E = \frac{1}{2} CV^2$$

where E is the energy density of the supercapacitor, C is the actual capacitance and V is the voltage window. Given:

$$\frac{1}{C} = \frac{1}{C_1} + \frac{1}{C_2}$$

Where C_1 and C_2 are capacitances of individual electrode. Normally, $C_1 = C_2 = C_E$ in symmetrical supercapacitors. Then $C = \frac{1}{2} C_E$. Dividing by $2m$, the total weight of two electrodes, we get

$$C_D = \frac{C}{2m} = \frac{1}{2} \cdot \frac{C_E}{2m} = \frac{1}{4} C_S$$

where C_D and C_S are capacitances specified to the device and individual electrode, respectively. Therefore,

$$E_D = \frac{1}{2} C_D V^2 = \frac{1}{8} C_S V^2$$

where E_D is the gravimetric energy density of the supercapacitor.

Supplementary Note 2

Synthesis of CNT arrays. The CNT arrays were synthesized through chemical vapour deposition. Silicon wafer was used as the substrate for catalyst. The catalyst, Fe (1.2 nm)/Al₂O₃ (5 nm) were successively sputtered on the silicon wafer by electron beam evaporation technique. The synthesis was carried out at 750 °C for 10 min. C₂H₄ (90 sccm) was used as carbon source, and a mixture of Ar (480 sccm) and H₂ (30 sccm) had been used as the carrier gas. The synthesized CNTs were multi-walled typically with a diameter of ~ 10 nm and the resulting CNT array was ~240 μm in height.

Supplementary Note 3

The spinability of CNT arrays. The spinability of CNT array is derived from the suitable interaction and entanglement among the neighbouring CNT bundles. The CNTs in the array are apt to aggregate into bundles due to van der Waals interactions among CNTs. In the growing process, the gas flow causes disturbance and redistribution of CNT bundles, which makes CNTs interpenetrated between two neighbouring bundles. When drawing a CNT bundle, the penetrated CNTs tend to aggregate at the end of the bundle which suffices for peeling off the proximate CNTs. Subsequently, CNT sheets are formed and drawn out continuously.

Supplementary Tables

Table S1. Summary of representative flexible batteries.

Flexible materials*	Cathode	Anode	Voltage (V)[†]	Ref.
Conductive paper	LiMn ₂ O ₄	Si	3	[S16]
CNT film	LiCoO ₂	Li ₄ Ti ₅ O ₁₂	2.3	[S17]
Graphene paper	V ₂ O ₅	graphene	2.0	[S18]
PDMS substrate	LiMn ₂ O ₄	Li ₄ Ti ₅ O ₁₂	2.4	[S19]
PDMS-CNT composite	LiCoO ₂	PDMS-CNT	3.4	[S20]
Cable-type configuration	LiCoO ₂	Ni-Sn	3.5	[S21]
Film electrode	LiFePO ₄	Li ₄ Ti ₅ O ₁₂	1.9	[S22]
PDMS substrate	LiCoO ₂	Li	4	[S23]
Carbon cloth/Al foil	LiCoO ₂	ZnCo ₂ O ₄	3.4	[S24]
Silicone substrate	LiCoO ₂	Li ₄ Ti ₅ O ₁₂	2.35	[S25]
Polymer Si nanowire	LiCoO ₂	Si	3.4	[S26]
Fibre electrodes	MnO ₂	Zn	1.5	[S27]
Paper-like electrodes	V ₂ O ₅ -PPy	Li foil	2.25	[S28]
CNT-coated papers	LiCoO ₂	Li ₄ Ti ₅ O ₁₂	2.25	[S29]
Graphene foam	LiFePO ₄	Li ₄ Ti ₅ O ₁₂	1.9	[S30]
Carbon textiles	LiCoO ₂	Si	3.24	[S31]
Polymer electrolytes	LiCoO ₂	Li ₄ Ti ₅ O ₁₂	2.3	[S32]
Cable-type configuration	O ₂	Zn	0.9	[S33]
Li ₄ Ti ₅ O ₁₂ nanosheet array	LiCoO ₂	Li ₄ Ti ₅ O ₁₂	2.3	[S34]
Li ₄ Ti ₅ O ₁₂ -CNT array	LiCoO ₂	Li ₄ Ti ₅ O ₁₂	2.3	[S35]
CNT-coated papers	LiCoO ₂	Li ₄ Ti ₅ O ₁₂	2.3	[S36]
Gum-like substrate	LiMn ₂ O ₄	Li ₄ Ti ₅ O ₁₂	2.4	[S37]

* Abbreviations: CNT: carbon nanotube; PDMS: polydimethylsiloxane;

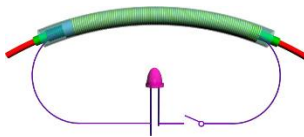
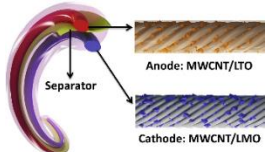
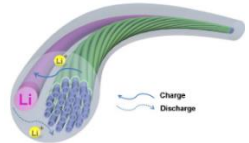
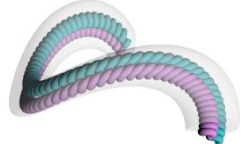
[†] The voltage here refers to the plateau voltage.

Table S2. Results of Brunauer-Emmett-Teller analysis of CMK-3 and CMK-3@S particles.

Sample	BET surface area (m²g⁻¹)	Pore volume (cm³g⁻¹)*	Pore size (Å)
CMK-3	1328.1	1.6360	43.50
CMK-3@S	64.5	0.0815	41.54

*The pore volume assigned to Barrett-Joyner-Halenda (BJH) adsorption cumulative volume of pores between 17 and 3000 Å.

Table S3. Performances of representative fibre-shaped rechargeable batteries.

Battery	Cathode	Anode	Voltage (V)	Capacity* (mAh g ⁻¹)	Cycles	Retention	Energy density* (Wh kg ⁻¹)	Ref.
	CNT-Si/CNT composite yarn	Li wire	0.3	2250	100	0.88	675	[S38]
	CNT-LiMn ₂ O ₄ hybrid fibre	CNT-Li ₄ Ti ₅ O ₁₂ hybrid fibre	2.5	138	100	0.85	345	[S39]
	CNT/Si composite fibre	Li wire	0.3	1670	50	0.32	501	[S40]
	Spring-like CNT-LiMn ₂ O ₄ hybrid fibre	Spring-like CNT-Li ₄ Ti ₅ O ₁₂ hybrid fibre	2.5	92.4	100	0.92	230	[S41]
	GO/CMK-3@S-CNT hybrid fibre	Li wire	2.1	714	100	0.54	1500	this study

*The capacity and energy density are specified to the weight of cathode.

Table S4. Electrochemical performances of representative sulphur cathodes.

Sulphur cathode	Initial capacity (C_0)	Rate (C)	Cycle	Retained capacity (C)	C_0/C	S%	Ref.
Graphene oxide	1000	0.1	50	954	0.954	46	[S42]
Porous carbon nanotube fibre	1146	0.1	20	1057	0.922	30	[S43]
CMK-3	1160	0.1	50	581	0.501	44.8	[S44]
Mesoporous carbon MC22	1050	0.1	50	613	0.584	66.5	[S44]
Mesoporous carbon MC12	1071	0.1	50	605	0.565	63.6	[S44]
Mesoporous carbon MC7	1195	0.1	50	607	0.508	52.4	[S44]
Polyaniline	755	0.1	100	837	1.109	49	[S45]
Double-shelled hollow carbon	1020	0.1	100	690	0.676	64	[S46]
Smaller sulphur molecules	1670	0.1	200	1149	0.688	32	[S47]
CMK-3@S in 7 mol/L LiTFSI	1041	0.2	100	770	0.740	57.4	[S1]
TiO ₂ @S	1460	0.2	100	680	0.466	50	[S48]
PAN & Mg _{0.6} Ni _{0.4} O	1545	0.1	100	1223	0.792	64	[S49]
N-doped mesoporous carbon	1100	0.1	100	800	0.727	56	[S50]
CNT flexible cathode	1109	0.1	100	740	0.667	65	[S51]
RGO wrapping carbon nanotube fibre	1047	0.1	50	694	0.663	33	[S52]
PPy coating CNT@S	1517	0.12	60	917	0.604	47.8	[S53]
Covalent organic framework	1497	0.1	50	762	0.509	34	[S54]
MOF: Ni ₆ (BTB) ₄ (BP) ₃	689	0.1	100	611	0.887	48	[S55]
Ti ₄ O ₇	1044	0.1	100	1034	0.990	51	[S56]

Supplementary References

- [S1] L. Suo, Y. Hu, H. Li, M. Armand, L. Chen, *Nat. Commun.* **2013**, *4*, 1481.
- [S2] S. H. Aboutalebi, R. Jalili, D. Esrafilzadeh, M. Salari, Z. Gholamvand, S. Aminorroaya Yamini, K. Konstantinov, R. L. Shepherd, J. Chen, S. E. Moulton, P. C. Innis, A. I. Minett, J. M. Razal, G. G. Wallace, *ACS Nano* **2014**, *8*, 2456-2466.
- [S3] S. Pan, H. Lin, J. Deng, P. Chen, X. Chen, Z. Yang, H. Peng, *Adv. Energy Mater.* **2015**, *5*, 1401438.
- [S4] X. Chen, H. Lin, P. Chen, G. Guan, J. Deng, H. Peng, *Adv. Mater.* **2014**, *26*, 4444-4449.
- [S5] X. Chen, H. Lin, J. Deng, Y. Zhang, X. Sun, P. Chen, X. Fang, Z. Zhang, G. Guan, H. Peng, *Adv. Mater.* **2014**, *26*, 8126-8132.
- [S6] J. Ren, W. Bai, G. Guan, Y. Zhang, H. Peng, *Adv. Mater.* **2013**, *25*, 5965-5970.
- [S7] Z. Zhang, J. Deng, X. Li, Z. Yang, S. He, X. Chen, G. Guan, J. Ren, H. Peng, *Adv. Mater.* **2015**, *27*, 356-362.
- [S8] H. Sun, X. You, Y. Jiang, G. Guan, X. Fang, J. Deng, P. Chen, Y. Luo, H. Peng, *Angew. Chem. Int. Ed.* **2014**, *53*, 9526-9531.
- [S9] Z. Cai, L. Li, J. Ren, L. Qiu, H. Lin, H. Peng, *J. Mater. Chem. A* **2013**, *1*, 258-261.
- [S10] H. Lin, L. Li, J. Ren, Z. Cai, L. Qiu, Z. Yang, H. Peng, *Sci. Rep.* **2013**, *3*, 1353.
- [S11] G. Sun, J. Liu, X. Zhang, X. Wang, H. Li, Y. Yu, W. Huang, H. Zhang, P. Chen, *Angew. Chem. Int. Ed.* **2014**, *53*, 12576-12580.
- [S12] G. Sun, X. Zhang, R. Lin, J. Yang, H. Zhang, P. Chen, *Angew. Chem. Int. Ed.* **2015**, doi: 10.1002/anie.201411533.
- [S13] D. Yu, K. Goh, H. Wang, L. Wei, W. Jiang, Q. Zhang, L. Dai, Y. Chen, *Nat. Nanotechnol.* **2014**, *9*, 555-562.
- [S14] L. Kou, T. Huang, B. Zheng, Y. Han, X. Zhao, K. Gopalsamy, H. Sun, C. Gao, *Nat. Commun.* **2014**, *5*, 3754.
- [S15] S. Zhang, N. Pan, *Adv. Energy Mater.* **2014**, doi: 10.1002/aenm.201401401.
- [S16] L. Hu, J. W. Choi, Y. Yang, S. Jeong, F. La Mantia, L.-F. Cui, Y. Cui, *Proc. Natl. Acad. Sci. USA* **2009**, *106*, 21490-21494.
- [S17] L. Hu, H. Wu, F. La Mantia, Y. Yang, Y. Cui, *ACS Nano* **2010**, *4*, 5843-5848.
- [S18] H. Gwon, H.-S. Kim, K. U. Lee, D.-H. Seo, Y. C. Park, Y.-S. Lee, B. T. Ahn, K. Kang, *Energy Environ. Sci.* **2011**, *4*, 1277-1283.
- [S19] Y. Yang, S. Jeong, L. Hu, H. Wu, S. W. Lee, Y. Cui, *Proc. Natl. Acad. Sci. USA* **2011**, *108*, 13013-13018.
- [S20] H. Lee, J.-K. Yoo, J.-H. Park, J. H. Kim, K. Kang, Y. S. Jung, *Adv. Energy Mater.* **2012**, *2*, 976-982.
- [S21] Y. H. Kwon, S.-W. Woo, H.-R. Jung, H. K. Yu, K. Kim, B. H. Oh, S. Ahn, S.-Y. Lee, S.-W. Song, J. Cho, H.-C. Shin, J. Y. Kim, *Adv. Mater.* **2012**, *24*, 5192-5197.

- [S22] Y. Liu, S. Gorgutsa, C. Santato, M. Skorobogatiy, *J. Electrochem. Soc.* **2012**, *159*, A349-A356.
- [S23] M. Koo, K.-I. Park, S. H. Lee, M. Suh, D. Y. Jeon, J. W. Choi, K. Kang, K. J. Lee, *Nano Lett.* **2012**, *12*, 4810-4816.
- [S24] B. Liu, J. Zhang, X. Wang, G. Chen, D. Chen, C. Zhou, G. Shen, *Nano Lett.* **2012**, *12*, 3005-3011.
- [S25] S. Xu, Y. Zhang, J. Cho, J. Lee, X. Huang, L. Jia, J. A. Fan, Y. Su, J. Su, H. Zhang, H. Cheng, B. Lu, C. Yu, C. Chuang, T.-i. Kim, T. Song, K. Shigeta, S. Kang, C. Dagdeviren, I. Petrov, P. V. Braun, Y. Huang, U. Paik, J. A. Rogers, *Nat Commun* **2013**, *4*, 1543.
- [S26] A. Vlad, A. L. M. Reddy, A. Ajayan, N. Singh, J.-F. Gohy, S. Melinte, P. M. Ajayan, *Proc. Natl. Acad. Sci. USA* **2012**, *109*, 15168-15173.
- [S27] X. Yu, Y. Fu, X. Cai, H. Kafafy, H. Wu, M. Peng, S. Hou, Z. Lv, S. Ye, D. Zou, *Nano Energy* **2013**, *2*, 1242-1248.
- [S28] L. Noerochim, J.-Z. Wang, D. Wexler, M. M. Rahman, J. Chen, H.-K. Liu, *J. Mater. Chem.* **2012**, *22*, 11159-11165.
- [S29] Q. Cheng, Z. Song, T. Ma, B. B. Smith, R. Tang, H. Yu, H. Jiang, C. K. Chan, *Nano Lett.* **2013**, *13*, 4969-4974.
- [S30] N. Li, Z. Chen, W. Ren, F. Li, H.-M. Cheng, *Proc. Natl. Acad. Sci. USA* **2012**, *109*, 17360-17365.
- [S31] B. Liu, X. Wang, H. Chen, Z. Wang, ChenDi, Y.-B. Cheng, C. Zhou, G. Shen, *Sci. Rep.* **2013**, *3*, 1622.
- [S32] K.-H. Choi, S.-J. Cho, S.-H. Kim, Y. H. Kwon, J. Y. Kim, S.-Y. Lee, *Adv. Funct. Mater.* **2014**, *24*, 44-52.
- [S33] J. Park, M. Park, G. Nam, J.-s. Lee, J. Cho, *Adv. Mater.* **2015**, *27*, 1396-1401.
- [S34] S. Chen, Y. Xin, Y. Zhou, Y. Ma, H. Zhou, L. Qi, *Energy Environ. Sci.* **2014**, *7*, 1924-1930.
- [S35] J. Liu, K. Song, P. A. van Aken, J. Maier, Y. Yu, *Nano Lett.* **2014**, *14*, 2597-2603.
- [S36] Z. Song, T. Ma, R. Tang, Q. Cheng, X. Wang, D. Krishnaraju, R. Panat, C. K. Chan, H. Yu, H. Jiang, *Nat Commun* **2014**, *5*, 3140.
- [S37] W. Weng, Q. Sun, Y. Zhang, S. He, Q. Wu, J. Deng, X. Fang, G. Guan, J. Ren, H. Peng, *Adv. Mater.* **2015**, *27*, 1363-1369.
- [S38] W. Weng, Q. Sun, Y. Zhang, H. Lin, J. Ren, X. Lu, M. Wang, H. Peng, *Nano Lett.* **2014**, *14*, 3432-3438.
- [S39] J. Ren, Y. Zhang, W. Bai, X. Chen, Z. Zhang, X. Fang, W. Weng, Y. Wang, H. Peng, *Angew. Chem. Int. Ed.* **2014**, *53*, 7864-7869.
- [S40] H. Lin, W. Weng, J. Ren, L. Qiu, Z. Zhang, P. Chen, X. Chen, J. Deng, Y. Wang, H. Peng, *Adv. Mater.* **2013**, *26*, 1217-1222.
- [S41] Y. Zhang, W. Bai, X. Cheng, J. Ren, W. Weng, P. Chen, X. Fang, Z. Zhang, H. Peng, *Angew. Chem. Int. Ed.* **2014**, *53*, 14564-14568.

- [S42] L. Ji, M. Rao, H. Zheng, L. Zhang, Y. Li, W. Duan, J. Guo, E. J. Cairns, Y. Zhang, *J. Am. Chem. Soc.* **2011**, *133*, 18522-18525.
- [S43] L. Ji, M. Rao, S. Aloni, L. Wang, E. J. Cairns, Y. Zhang, *Energy Environ. Sci.* **2011**, *4*, 5053-5059.
- [S44] X. Li, Y. Cao, W. Qi, L. V. Saraf, J. Xiao, Z. Nie, J. Mietek, J.-G. Zhang, B. Schwenzer, J. Liu, *J. Mater. Chem.* **2011**, *21*, 16603-16610.
- [S45] L. Xiao, Y. Cao, J. Xiao, B. Schwenzer, M. H. Engelhard, L. V. Saraf, Z. Nie, G. J. Exarhos, J. Liu, *Adv. Mater.* **2012**, *24*, 1176-1181.
- [S46] C. Zhang, H. B. Wu, C. Yuan, Z. Guo, X. W. Lou, *Angew. Chem. Int. Ed.* **2012**, *51*, 9592-9595.
- [S47] S. Xin, L. Gu, N.-H. Zhao, Y.-X. Yin, L.-J. Zhou, Y.-G. Guo, L.-J. Wan, *J. Am. Chem. Soc.* **2012**, *134*, 18510-18513.
- [S48] Q. Li, Z. Zhang, K. Zhang, L. Xu, J. Fang, Y. Lai, J. Li, *J. Solid State Electrochem.* **2013**, *17*, 2959-2965.
- [S49] Y. Zhang, Y. Zhao, A. Yermukhambetova, Z. Bakenov, P. Chen, *J. Mater. Chem. A* **2013**, *1*, 295-301.
- [S50] J. Song, T. Xu, M. L. Gordin, P. Zhu, D. Lv, Y.-B. Jiang, Y. Chen, Y. Duan, D. Wang, *Adv. Funct. Mater.* **2014**, *24*, 1243-1250.
- [S51] K. Jin, X. Zhou, L. Zhang, X. Xin, G. Wang, Z. Liu, *J. Phys. Chem. C* **2013**, *117*, 21112-21119.
- [S52] S. Lu, Y. Cheng, X. Wu, J. Liu, *Nano Lett.* **2013**, *13*, 2485-2489.
- [S53] C. Wang, W. Wan, J.-T. Chen, H.-H. Zhou, X.-X. Zhang, L.-X. Yuan, Y.-H. Huang, *J. Mater. Chem. A* **2013**, *1*, 1716-1723.
- [S54] H. Liao, H. Ding, B. Li, X. Ai, C. Wang, *J. Mater. Chem. A* **2014**, *2*, 8854-8858.
- [S55] J. Zheng, J. Tian, D. Wu, M. Gu, W. Xu, C. Wang, F. Gao, M. H. Engelhard, J.-G. Zhang, J. Liu, J. Xiao, *Nano Lett.* **2014**, *14*, 2345-2352.
- [S56] Z. W. Seh, J. H. Yu, W. Li, P.-C. Hsu, H. Wang, Y. Sun, H. Yao, Q. Zhang, Y. Cui, *Nat. Commun.* **2014**, *5*, DOI: 10.1038/ncomms6017.